MARINE ROBOTS

Plasticized electrohydraulic robot autopilots in the deep sea

Guorui Li[1,2,3,4]*, Peng Shen[1,2,3], Tuck-Whye Wong[5], Mingyu Liu[1,2], Zhenxiang Sun[1,2], Xinyu Liu[2], Yongzai Chen[2], Xianghan Wang[1,2], Hao Zhang[6], Bingxu Hu[2], Deli Chen[1,2], Zhihan Zhang[1,2], Chao Zhang[2], Rongchen Wang[2], Wenhao Zhang[2], Shuai Nie[2], Xinyue Zhang[2], Jie-Wei Wong[5], Haofei Zhou[5], Wenbo Li[7], Hao Wang[1,2,4], Qian Zhang[1,2,4], Shenlong Wang[8], Zhiwen Yu[3,9], Hai Li[10], Hongyu Zhao[11], Qingyun Zeng[1], Shiping Wang[1], Zhilong Huang[5], Cong Ye[6], A-Man Zhang[1], Tiefeng Li[5,12,13]*

Soft robots, with their compliant bodies, minimal environmental disturbance, and ability to withstand ambient pressures, offer promising solutions for deep-sea exploration. However, a common challenge of stiffening in soft materials impairs their effective actuation in harsh conditions. In this work, we integrated a liquid dielectric plasticizer within an electrohydraulic soft robot, serving dual critical functions as a softening agent to maintain the softness of the polymer shell and an electrohydraulic fluid for efficient actuation. In addition, by using the surrounding seawater as alternating electrodes, we prevented charge retention in dielectric layers, enabling sustained actuation performance. Field tests at depths of ~1360, 3176, and ~4071 meters confirmed the robot's ability to sense the environment, navigate complex trajectories, and withstand unsteady disturbances. Our work offers a generalized and straightforward framework for developing soft materials tailored for deep-sea applications, paving the way for soft robots to execute real-world missions.

INTRODUCTION

The deep ocean remains one of Earth's least explored regions, presenting extreme challenges because of immense pressures, near-freezing temperatures, and perpetual darkness. Conventional deep-sea mobile robots, typically composed of rigid components, have been the primary tools for oceanic navigation (*1*–*4*). However, these "hard" machines encounter common challenges in extreme underwater environments, including increased weight, limited adaptability, and disturbance to deep-sea creatures. These limitations highlight the need for innovative alternatives. Soft robots emerge as a promising solution to revolutionize deep-sea exploration, offering inherent pressure resilience, fully soft-bodied structures, and gentle navigation that minimizes environmental disturbance (*5*–*8*). With their adaptability and nonintrusive design, mobile soft robots have the potential to enable more sustainable and insightful oceanic research (*9*–*11*).

Recent advances have explored various deep-sea actuation mechanisms, including hydraulics for delicate manipulation (*12*–*16*), shape memory alloy (SMA)–based machines (*17*, *18*), and a dielectric elastomer (DE)–driven flapping robot (*19*). Hydraulic systems, although effective because of their high energy density and multimodal deformations, necessitate the use of bulky pumps and pressure-regulating components, complicating their integration into compact and flexible designs (*12*–*16*). SMAs, although capable of large actuations, suffer from poor energy efficiency and slow actuation speeds because of the reliance on thermal heating and cooling processes (*17*). Although DE-based actuators can be powered and controlled in untethered settings, the need for prestretching in materials restricts such robots to simple deformations, preventing more sophisticated movements for practical deep-sea tasks (*19*, *20*). Alternatively, soft electrohydraulics, which facilitate diverse propulsive modes and pressure resilience through the redistribution of internal dielectric liquids without requiring an external deep-sea pump (*21*–*28*), are positioned as another promising candidate for powering future deep-sea mobile soft robots.

One of the key challenges in designing deep-sea mobile soft robots with effective and compact actuation lies in the common stiffening of soft materials, particularly for stimuli-responsive applications, caused by the extreme low temperatures and high pressures (*29*–*35*). Along with the chain entanglement, the flexibility and resilience of polymeric materials are severely compromised. As a result, the core concept of "softness" is undermined, leading to decreased actuation and limited locomotion capabilities of robots (*19*, *36*). Although researchers have attempted to chemically modify DEs to lower their glass transition temperatures (T_g) and reduce the stiffness under deep-sea conditions, these methods pose a scalability challenge and introduce complexities in material processing, limiting their practical application and long-term viability (*19*, *37*). Plasticization is a well-established approach in material science, widely used to reduce the stiffness of polymeric materials by increasing polymer chain mobility (*38*–*40*). When a polymer is exposed to a plasticizer, the plasticizer molecules penetrate the polymer matrix, disrupting intermolecular forces and allowing greater segmental

[1]College of Shipbuilding Engineering, Harbin Engineering University, Harbin, 150001, China. [2]Qingdao Innovation and Development Base, Harbin Engineering University, Qingdao, 266000, China. [3]National Key Laboratory of Autonomous Marine Vehicle Technology, Harbin Engineering University, Harbin, 150001, China. [4]Zhishui Lab, Harbin Engineering University, Harbin, 150001, China. [5]Center for X-Mechanics, Zhejiang University, Hangzhou, 310027, China. [6]China Ship Scientific Research Center, Wuxi, 214082, China. [7]School of Aerospace Engineering and Applied Mechanics, Tongji University, Shanghai, 200092, China. [8]School of Mechanical Engineering, University of Shanghai for Science and Technology, Shanghai, 200093, China. [9]School of Computer Science, Northwestern Polytechnical University, Xi'an, 710129, China. [10]School of Electronics and Information Engineering, Hangzhou Dianzi University, Hangzhou, 310018, China. [11]Guangdong Institute of Intelligent Unmanned System (Nansha), Guangzhou, 511400, China. [12]Institute of Fundamental and Transdisciplinary Research, Zhejiang University, Hangzhou, 310058, China. [13]State Key Laboratory of Ocean Sensing, Zhejiang University, Hangzhou, 310058, China.
*Corresponding author. Email: grli@hrbeu.edu.cn (G.L.); litiefeng@zju.edu.cn (T.L.)

movement. This mechanism effectively lowers the polymer's elastic modulus, maintaining flexibility and deformation capability even at frigid temperatures and high pressures.

Here, we introduced the integration of a dielectric plasticizer within soft electrohydraulics, serving dual functions as the electrohydraulic fluid facilitating actuation and force transmission and a softening agent for the polymer casing (Fig. 1, A to C). This design strategy preserved the softness and flexibility of the polymer shell, ensuring sufficient actuation performance of the soft robot under the extreme conditions of 110 MPa and 2°C (Fig. 1, D to F). Our approach presents a straightforward strategy to maintain large deformations in electrohydraulics and can be generalized to a wide range of soft materials tailored for deep-sea applications. In addition, by using the surrounding seawater as alternating positive and negative electrodes, our design eliminated the need for fully underwater insulation of each electrode and prevented charge retention in dielectric layers, thereby ensuring prolonged actuation efficiency. These features enhanced the locomotion capabilities and overall functionality of our deep-sea soft robot, enabling reliable operation under hydrostatic pressures up to 110 MPa, conditions akin to those at the bottom of the Mariana Trench. Field tests at depths of ~1360, 3176, and ~4071 m demonstrated the robot's ability to navigate complex trajectories, perform multilocomotion maneuvers, autonomously sense and regulate altitudes near the seabed, and withstand sizeable disturbances. Our work provides a versatile framework for developing advanced soft materials and machines, potentially inspiring future robots designed for practical deep-sea tasks.

RESULTS

Deep-sea soft electrohydraulic actuation

Electrohydraulic actuators represent a promising solution for innovative deep-sea soft robots because of their abilities to generate rapid and large deformation without the need for cumbersome external pumps (*21*–*28*). In our design, we capitalized on the above advantages to propel our soft robot for deep-sea missions. Drawing inspiration from the structure and propulsion mechanism of undulating caudal fins, we developed a soft robotic fish that incorporated paired arrays of electrohydraulic units as muscle laminates, a silicone frame as the supporting skeleton, and a thin silicone sheet as the fin. At the heart of the electrohydraulic system was the muscle laminate, which consisted of two flexible polyethylene (PE) dielectric films sealed together, encapsulating displaceable units of dielectric liquids. A conductive fabric, enclosed within a waterproof PE layer, served as the electrode. The muscle laminates, once integrated with the silicone framework, enabled the robot's electrohydraulic actuation, forming the key component of its propulsion system. The detailed fabrication process is illustrated in Fig. 2A and fig. S1.

Recently, electrohydraulics have been used to fabricate elegant soft robots such as jumpers (*26*, *28*), jellyfish (*23*), and swimmers (*27*), showcasing a wide range of possibilities through different material selections and structural designs. Nevertheless, primary challenges remain in designing deep-sea soft machines capable of effective actuation. In particular, the increased viscosity of dielectric liquids (*41*) and stiffening of polymeric shells at low temperatures and high pressures severely impede the quick flow of the dielectric liquids and hinder the large deformations needed for effective actuation. To address these critical challenges, we measured the voltage-induced

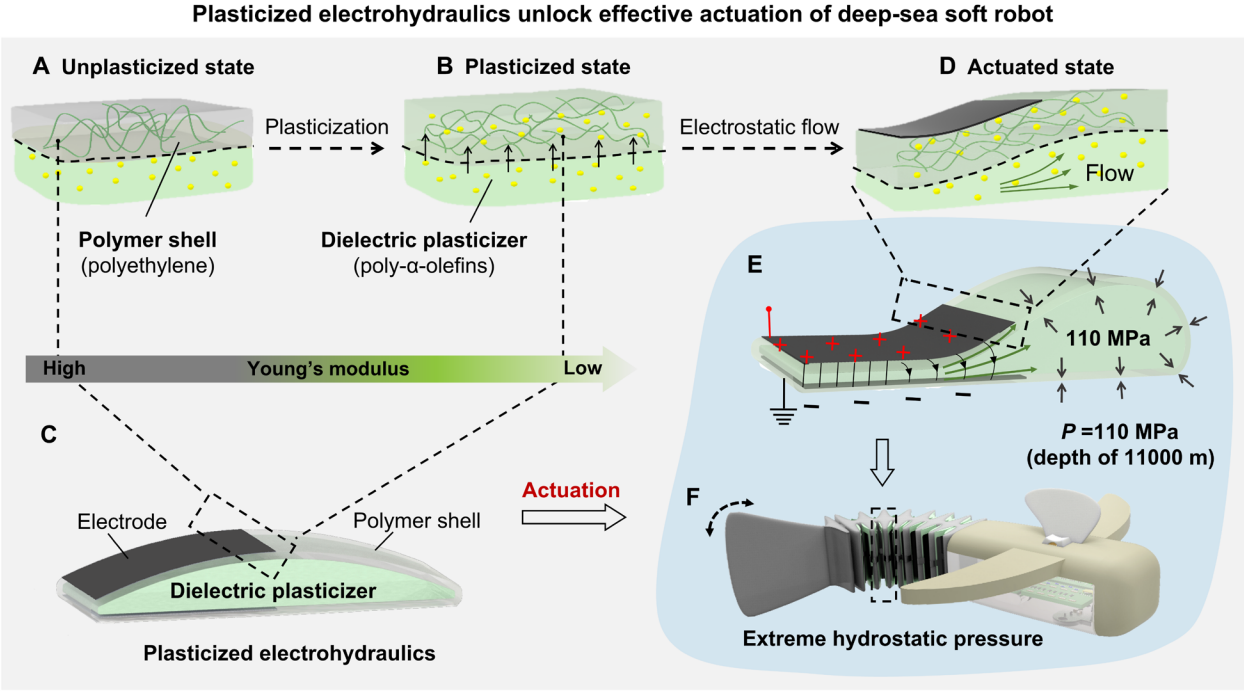

Fig. 1. Deep-sea soft robot driven by plasticized electrohydraulics. (**A** to **C**) The dielectric plasticizer is encapsulated and defused in a polymer layer, which serves dual functions as the electrohydraulic fluid and as a softening agent for the polymer in the soft electrohydraulics. (**D** to **F**) As a voltage is applied on the electrode, the induced electrostatic force displaces the internal liquid dielectric plasticizer, thereby deforming the electrohydraulics and enabling a deep-sea soft robot to perform fish-like locomotion, even under a hydrostatic pressure of 110 MPa.

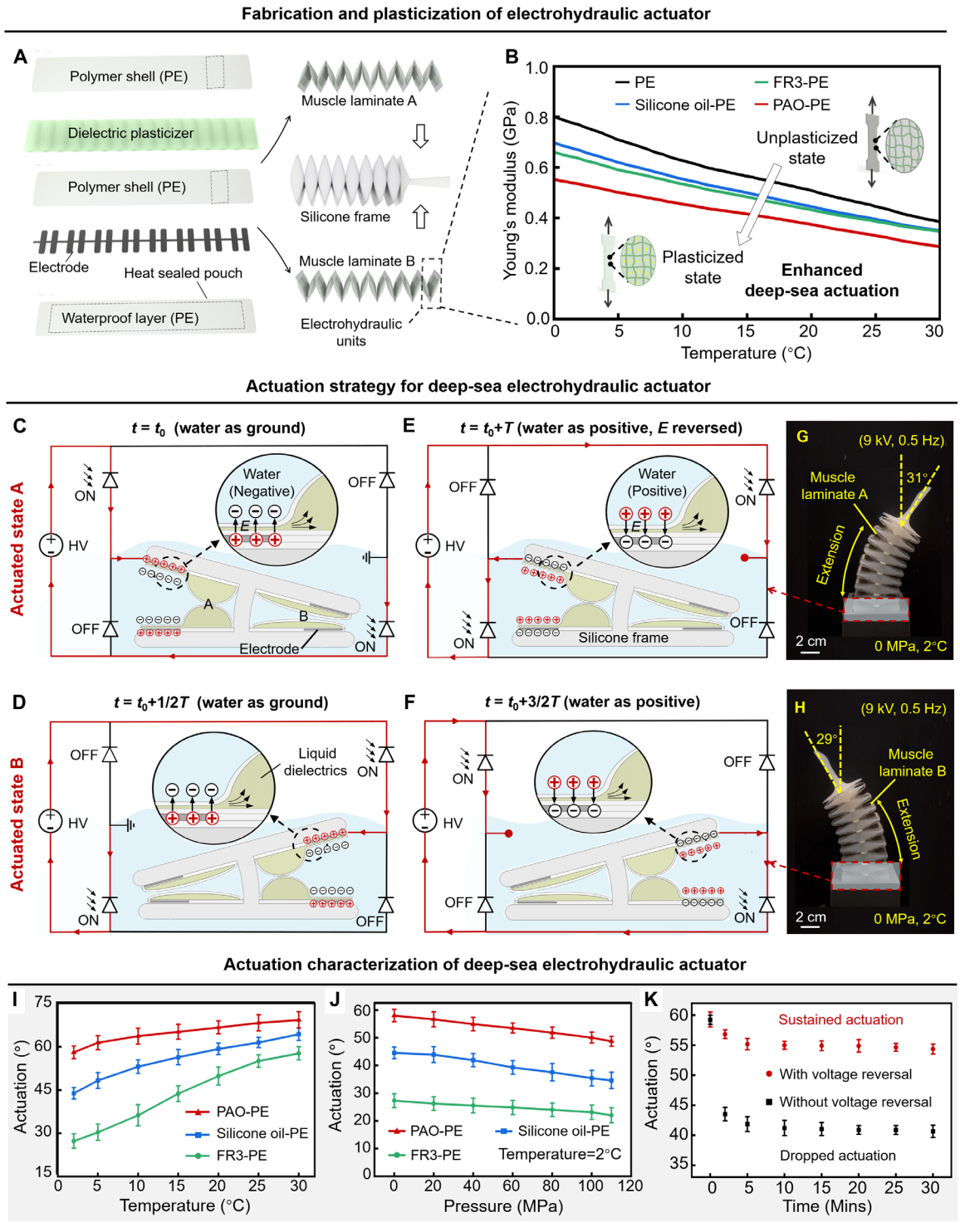

Fig. 2. Design and actuation principle of plasticized deep-sea electrohydraulics. (**A**) The design and assembly of the electrohydraulic actuator, which integrated an array of electrohydraulic units as the muscle laminates and a silicone framework as the supporting skeleton. Each electrohydraulic unit comprises a flexible pouch, made of a PE shell and filled with a liquid dielectric plasticizer, and a compliant electrode. (**B**) DMA testing results of PE films and those immersed 48 hours in FR3, dimethyl silicone oil, or PAO. (**C**) At the first stage, HV was applied to muscle laminate A, driving ions toward the electrodes and causing the skeleton to bend into state A. (**D**) After that, the voltage was applied to muscle laminate B, bending the skeleton into state B. The surrounding water acts as the electric ground. (**E** and **F**) In the next phase, a reversed voltage was applied alternately to muscle laminates A and B, eliminating residual charges and inducing cyclic bending. The surrounding water serves as the positive electrode. t_0 is defined as the beginning of the cycle in the actuated state, and T represents the time required for one full bending cycle. (**G** and **H**) Snapshots of the actuation state A and state B. Scale bars, 2 cm. (**I** and **J**) Actuation characterization of actuators made of PAO with PE, FR3 with PE, or dimethyl silicone oil with PE under various hydrostatic pressures and temperatures. Error bars represent SD ($n = 3$). (**K**) Actuation characterization in contrast with the design without reversed voltage. Error bars represent SD ($n = 3$).

deformation (bending angle) of several actuators under varying temperatures and hydrostatic pressures. Actuators fabricated using dimethyl silicone oil or Envirotemp transformer oil (FR3) as the dielectric liquid and PE as the polymer shell exhibited a substantial decline in performance. At 9 kV and 0.5 Hz, the actuation dropped sharply from 64.3° to 34.6° for dimethyl silicone oil with PE and from 57.7° to 22.1° for FR3 with PE, when experimental conditions shifted from 0 MPa and 30°C to 110 MPa and 2°C. The selection of FR3 and silicone oil as experimental groups was based on their prevalent use as dielectric liquids in electrohydraulic actuators in prior research (*22*–*25*). The observed actuation reduction is insufficient to propel the soft robot in a deep-sea environment. Further dynamic thermomechanical analysis (DMA) and rheological tests revealed that the decreased performance stemmed from the notable increase in stiffness of PE films (Fig. 2B) and the viscosity of the dielectric liquids under such conditions (fig. S2). More details about the DMA test and viscosity characterization are illustrated in figs. S2 and S3.

To refine the design principle for deep-sea electrohydraulics, we herein introduced the use of liquid dielectric plasticizer with a lower viscosity to address the aforementioned obstacle, which served dual critical roles: as a softening agent for the polymer shell to preserve its softness and alleviate stiffening and as an efficient electrohydraulic fluid for force transmission under deep-sea conditions. Specifically, poly-α-olefin (PAO) was selected for its low viscosity at deep-sea temperatures (fig. S2) as well as its chemical compatibility and high plasticizing ratio of ~8% with PE shell materials, compared with ~1.2% for silicone oil and ~3.4% for FR3 (fig. S4). After 48 hours of immersion in PAO, the plasticizer achieved a uniform and saturated distribution within the polymer matrix. As a result, the Young's modulus of PE was substantially reduced (Fig. 2B), enhancing the voltage-induced actuation even under the pressures and temperatures akin to deep-sea conditions. Given an identical actuating voltage of 9 kV at 0.5 Hz, this design maintained an actuating angle of 48.8° at 110 MPa and 2°C, which was sufficient to power the robot's locomotion and enable it to withstand environmental disturbances during deep-sea swimming.

Figure 2 (C to F) presents the actuation mechanism of the soft robot. Electrohydraulic soft actuators, especially in aquatic environments, typically require full insulation to avoid safety risks, such as electric breakdown caused by high operating voltages. Although previous studies have shown that surrounding water can be used as the electric ground in such situations, performance degradation still occurs because of charge retention in dielectric layers and electroadhesion of the polymer shell. Our approach overcame this limitation by using the surrounding water as alternating positive and negative electrodes. The cyclic voltage reversal strategy effectively mitigated charge retention, ensuring sustained performance during deep-sea operations. In the initial stage, a high voltage (HV) was applied to muscle laminate A, driving ions toward the electrodes and displacing the dielectric liquid, causing the skeleton to bend into state A (Fig. 2C). Subsequently, the voltage was applied to muscle laminate B, resulting in a similar displacement of the dielectric liquid and bending the skeleton into state B (Fig. 2D). Here, the surrounding water acted as the electric ground. In the next phase, a reversed voltage was applied alternately to the electrodes of muscle laminates A and B, generating an opposite electric field that eliminated charge retention in the polymer shell (Fig. 2, E and F). In this phase, the surrounding water functioned as the positive electrode. The periodic voltage reversal drove the cyclic deformation of the electrohydraulic muscle laminates, generating thrust and enabling the fish-like locomotion of the robot (Fig. 2, G and H). This voltage reversal approach addressed the issue of actuation degradation due to charge retention in PE layers over time. As a result, we substantially enhanced the robot's ability to maintain effective actuation over prolonged periods in deep-sea environments.

We conducted extensive tests to characterize the performance of aforementioned electrohydraulic soft actuators under various temperatures and hydrostatic pressures (Fig. 2, I and J). Here, the actuation refers to the addition of actuation angles in actuated states A and B. The performance of electrohydraulic actuators is determined by an interdependent effect between the plasticization on the polymer shell and the viscosity of the dielectric plasticizer. Whereas plasticization enhances the softness and deformability of the shell, viscosity influences the dynamic flow and redistribution of the dielectric liquid. Our experimental results revealed that the optimal material selection requires accommodation of both of these two factors, as exemplified by PAO, which achieved superior actuation performance because of its strong plasticization effect on PE and favorable low viscosity. In addition, given the identical experimental condition of 2°C, the actuator with cyclic voltage reversal of 9 kV at 0.5 Hz maintained a durable bending angle of 54.3°, whereas an actuator without this reversal exhibited a substantial decline in actuation, decreasing from 59.2° to 43.5° in 2 min (Fig. 2K). These results highlighted the critical role of using a dielectric plasticizer with a favorable combination of a lower viscosity and a higher plasticizing effect on polymer shell, in conjunction with cyclic voltage reversal to enhance the electromechanical performance of deep-sea electrohydraulic actuators and soft robots.

Soft robot design

The prototype of our soft robot, shown in Fig. 3A, measures 32 cm in length and 18 cm in wingspan and weighs 670 g. Its design features an undulating tail for deep-sea propulsion, two pectoral fin–like buoyancy modules for stabilization and antirolling, an electromagnetic dorsal fin paired with an optical sensing module for closed-loop altitude adjustment, and an integrated camera for underwater investigation. On the basis of the preprogrammed set point of altitude, the distance between the soft robot and the seabed can be continuously monitored by the optical sensor and regulated by the dorsal fin (as shown in fig. S5). In addition, the robot was equipped with an onboard electronic system that provides power and control. This lightweight system integrates a micro control unit (MCU), an optical distance sensor, a multichannel HV amplifier, a lithium-ion battery, and infrared (IR) remote control circuits. To mitigate the shear stress between the interfaces, all of the electronics were arranged in a decentralized manner (*19*) and placed inside a 3D-printed mold. The silicone precursor was then poured into the mold and cured to fully encapsulate the electronics and form the soft electronic pod. It is also noteworthy that the optical sensing module was accommodated in a fluid-filled enclosure, which eliminated the internal air gap to ensure operating under extreme hydrostatic pressures. Furthermore, a miniature camera was encapsulated in the epoxy and integrated into the soft robot for in situ investigations. The detailed fabrication process is illustrated in figs. S6 and S7. The undulating tail was powered by electrohydraulic muscle laminates, with a HV amplifier boosting the battery voltage from 7.4 V to a maximum of 9 kV across two independently controlled channels. The MCU, along with HV opto-diodes, enabled the periodic switching of positive and negative electrodes, preventing charge

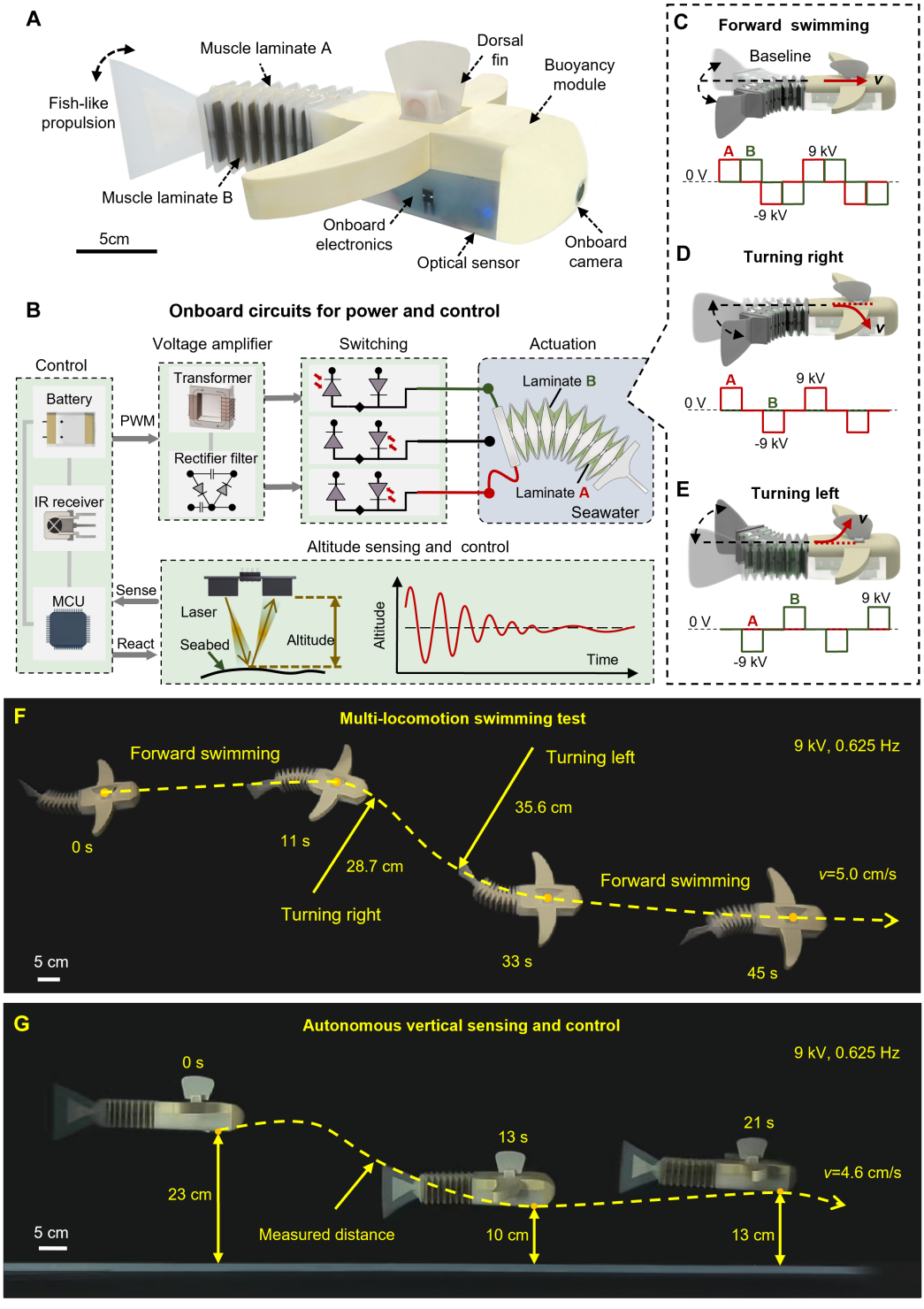

Fig. 3. Design and swimming test in the lab. (**A**) The overall design and prototype of this soft robot with a body length of 32 cm. Scale bar, 5 cm. (**B**) Schematic of circuit and system integration of the robot. (**C** to **E**) The programmed actuation and locomotion corresponding to the sequenced signal on the muscle laminates. (**F**) The top-view live snapshots of this robot including forward swimming and turning. Scale bar, 5 cm. (**G**) The side-view live snapshots with vertical sensing and control. Scale bar, 5 cm.

retention and sustaining large actuation in deep-sea conditions (Fig. 3B). The programmed undulating motion and locomotion corresponding to the sequenced signals applied to the muscle laminates are illustrated in Fig. 3 (C to E). By synchronizing voltage signals across both channels, the internal fluid redistribution deformed the fishtail, producing a cyclic bending motion that propelled the robot forward. By applying cyclic voltage to only one actuator, the robot can steer left or right, offering high maneuverability. More details about the electronic circuitry are provided in fig. S8.

Swimming experiments

Initial experiments to evaluate the robot's swimming performance were conducted in a laboratory tank. When actuated with the preprogrammed voltages, the robot transitioned between two distinct actuation states, thereby demonstrating a variety of movements, including forward swimming at a speed of 5.0 cm/s, right turns with a radius of 28.7 cm, and left turns with a radius of 35.6 cm (9 kV and 0.625 Hz; Fig. 3F). These results illustrate the robot's high agility, as further shown in movie S1. In addition, we tested its vertical sensing and control capabilities, where the soft robot autonomously measured its vertical position and maintained variable distances from the tank bottom, ranging from 23 to 10 cm, showcasing its ability to react and adapt to its environment (Fig. 3G and movie S1).

In addition, we further validated the robot's performance under high hydrostatic pressure conditions. The robot was released by a motor-driven, freely rotatable rod (Fig. 4A). Figure 4 (B to G) records snapshots of swimming experiments where the robot was actuated with a preprogrammed voltage (9 kV and 0.625 Hz) at a

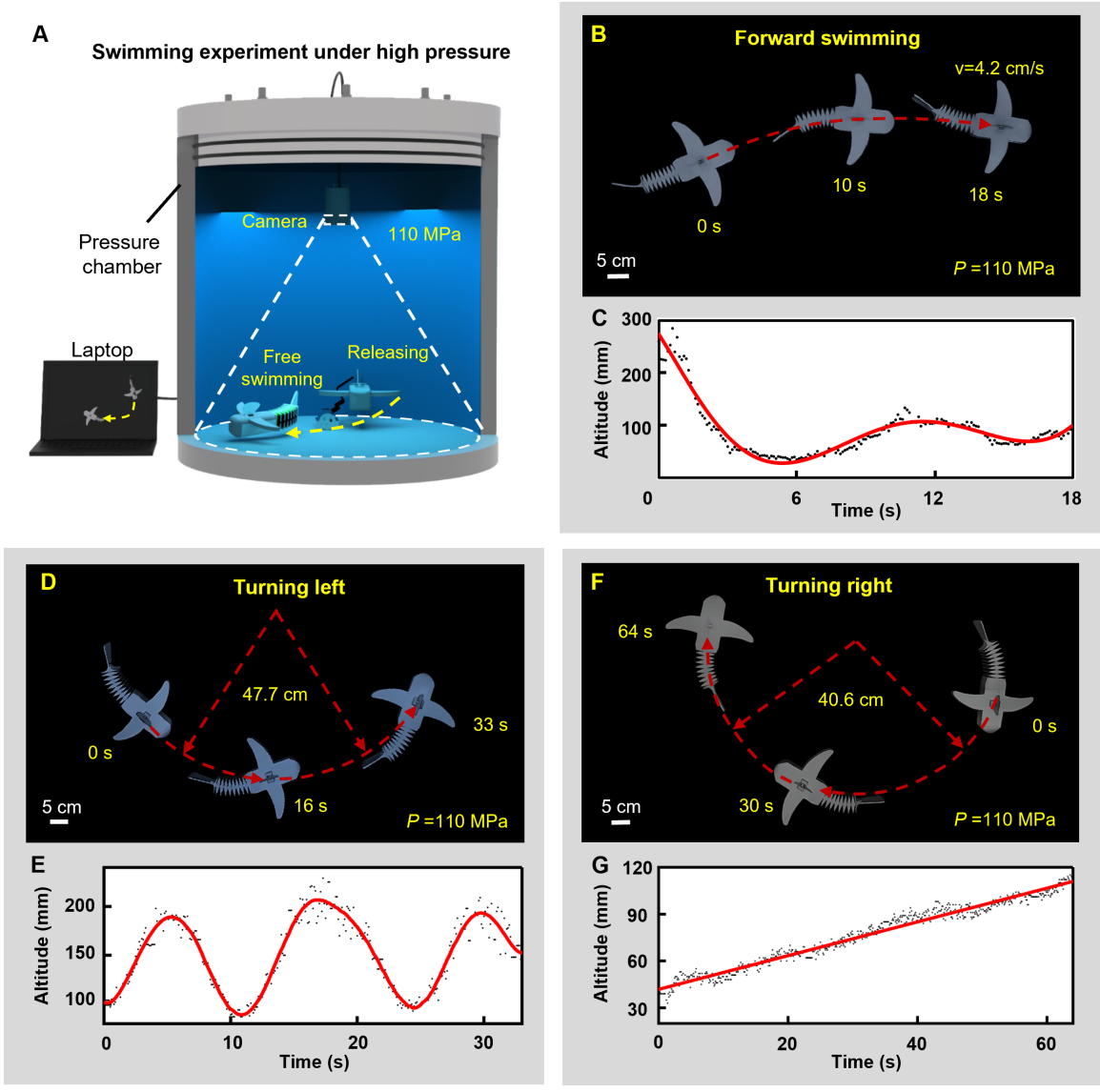

Fig. 4. Swimming experiments in a pressure chamber. (**A**) Experimental setups, where the robot was released by a motor and its swimming trajectory was recorded with a camera, under a hydrostatic pressure of 110 MPa (corresponding to the pressure at a depth of 11,000 m). (**B** and **C**) Forward swimming snapshots and real-time altitude data of the soft robot. (**D** and **E**) Left turning snapshots and real-time altitude data of the soft robot. (**F** and **G**) Right turning snapshots and real-time altitude data of the soft robot.

hydrostatic pressure of 110 MPa. Overall, the robot achieved forward swimming locomotion with a speed of 4.2 cm/s (Fig. 4B) and completed left turns with a radius of 47.7 cm (Fig. 4D) and right turns with a radius of 40.6 cm (Fig. 4F). Furthermore, the dynamic altitude data were obtained from the integrated optical sensor and confirmed the robot's responsiveness to its environmental changes. Powered by a single lithium-ion battery, the robot could swim continuously for at least 2 hours under an extreme pressure of 110 MPa and a temperature between 0° and 5°C. The measured operation time could be degraded because of the freezing temperature and extreme pressures. Further attempts to advance batteries with high-pressure and low-temperature resilience could potentially enhance the endurance of the robot. In future designs and applications of deep-sea soft robots, the optimization of swimming speed and working frequency should be a key consideration. Several potential strategies include modifying the mechanical stiffness of the silicone frameworks for improved structural response, selecting a favorable dielectric plasticizer to enhance dynamic actuation performance, refining the hydrodynamic streamlining of the soft robot body, and using a polymer shell with a rapid dynamic response. More details about the experimental setup in the pressure chamber are shown in fig. S9.

Navigating complex trajectories in deep sea

Our soft robot successfully demonstrated multilocomotion, free-swimming trajectories during a field test conducted at a depth of 3176 m in the South China Sea. Figure 5A illustrates the schematic and experimental setup. The robot was deployed near the seabed by a deep-sea remotely operated vehicle (ROV) and powered by an onboard lithium-ion battery (800 mAh) coupled with a HV amplifier (AC voltage of 9 kV at 0.625 Hz). Equipped with an optical distance sensor, the robot was capable of precisely sensing and responding to its environment, continuously monitoring and regulating its desired altitude to the uneven seabed, even in turbid conditions.

The field test was conducted in three stages to comprehensively assess the robot's performance and capabilities. In the first stage, the robot executed a sequence of complex deformations and multilocomotion, including forward swimming, turning, and heaving. By adjusting the baseline deflection angle of its simple-structured tail, the robot completed an S-shaped trajectory, demonstrating its

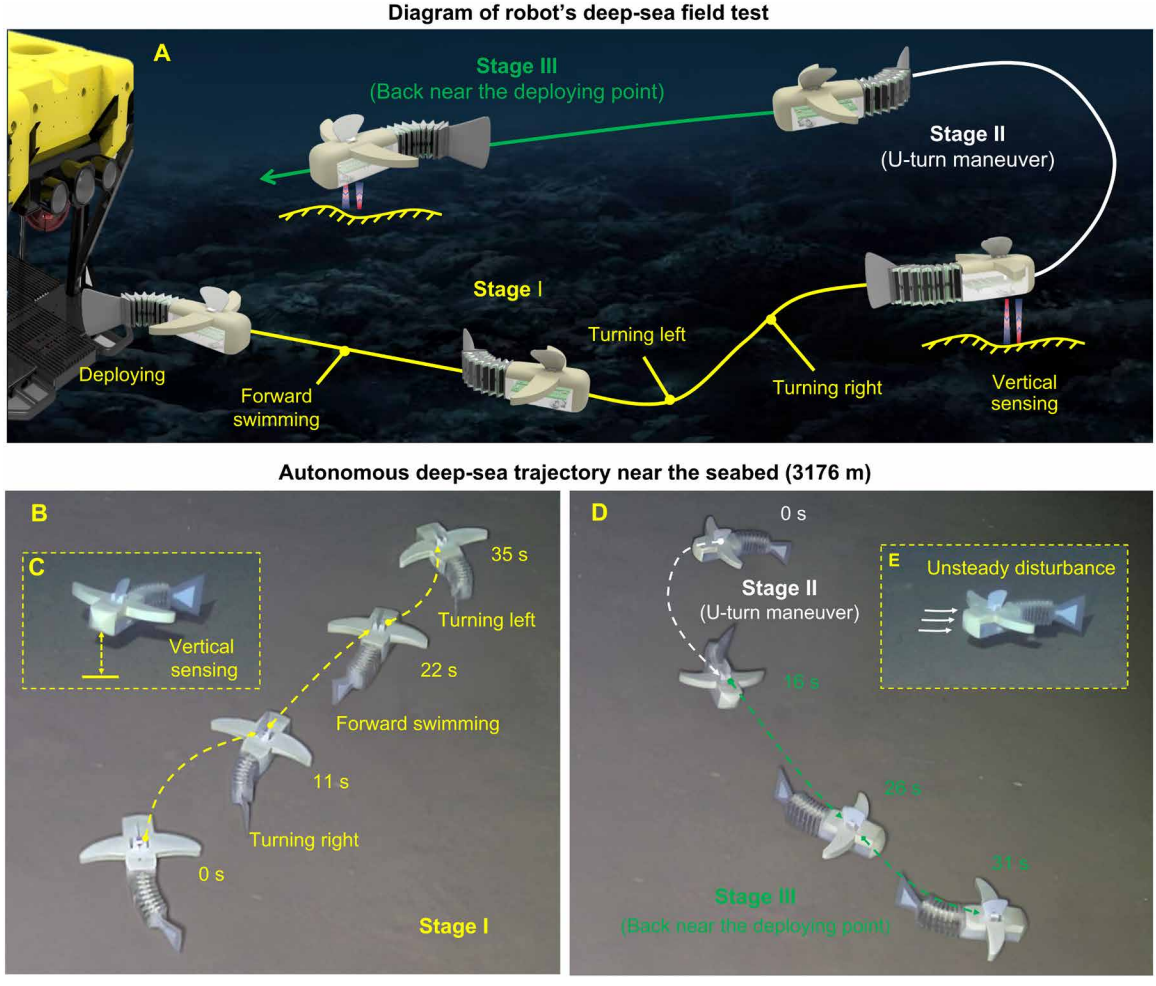

Fig. 5. Navigating complex trajectories in the deep sea. (**A**) Diagram of the deep-sea field test, where the robot was deployed to a depth of 3176 m by a deep-sea ROV, and presented in three experimental stages. (**B** and **C**) At stage one, the robot demonstrated multilocomotion, including forward swimming, turning, and altitude controlling through integrated sensing. (**D** and **E**) In the second and third stages, the robot successfully performed a U-turn maneuver in turbulent conditions, followed by navigating back near the deploying point. (B) to (E) are snapshot images from the field test.

ability to perform sophisticated maneuvers (Fig. 5, B and C). In the second stage, the robot performed a U-turn maneuver, even in turbulent conditions, highlighting its adaptability and precise control in unpredictable environments (Fig. 5, D and E). Last, in the third stage, the robot swam in the opposite direction from its release point, navigating back through the environment it had just traversed, which demonstrated its ability to reverse course—a critical function for practical deep-sea exploration tasks (Fig. 5D). The robot's locomotor capabilities were further reinforced by its ability to withstand sizeable disturbances, achieving a downstream speed of ~3.1 cm/s, an upstream speed of ~6.2 cm/s, and a turning radius of ~31.2 cm. These metrics confirmed its robustness and represented an advancement over our previous mobile robot (*19*). The observed speeds and turning radius may be influenced by the dynamic view of the camera and the unsteady flow conditions in the deep sea. Detailed descriptions of the field experiments are provided in fig. S10 and movie S2.

Deep-sea swimming test

To further evaluate the endurance and long-term robustness of our soft robot in real-world deep-sea conditions, swimming tests were conducted at various depths. First, the robot was deployed by a deep-sea ROV at an approximate depth of 1360 m. This robot completed a forward swimming locomotion, along with smooth turns and circular movements in turbulent conditions (Fig. 6, A to C, and movie S3). This robot can sustain long-endurance deep-sea operations for up to 1.5 hours. These results highlighted the robot's capacity for prolonged operation in deep-sea environments, essential for practical exploration tasks. Moreover, the portable robot was further tested at a greater depth of ~4071 m, where it was released from

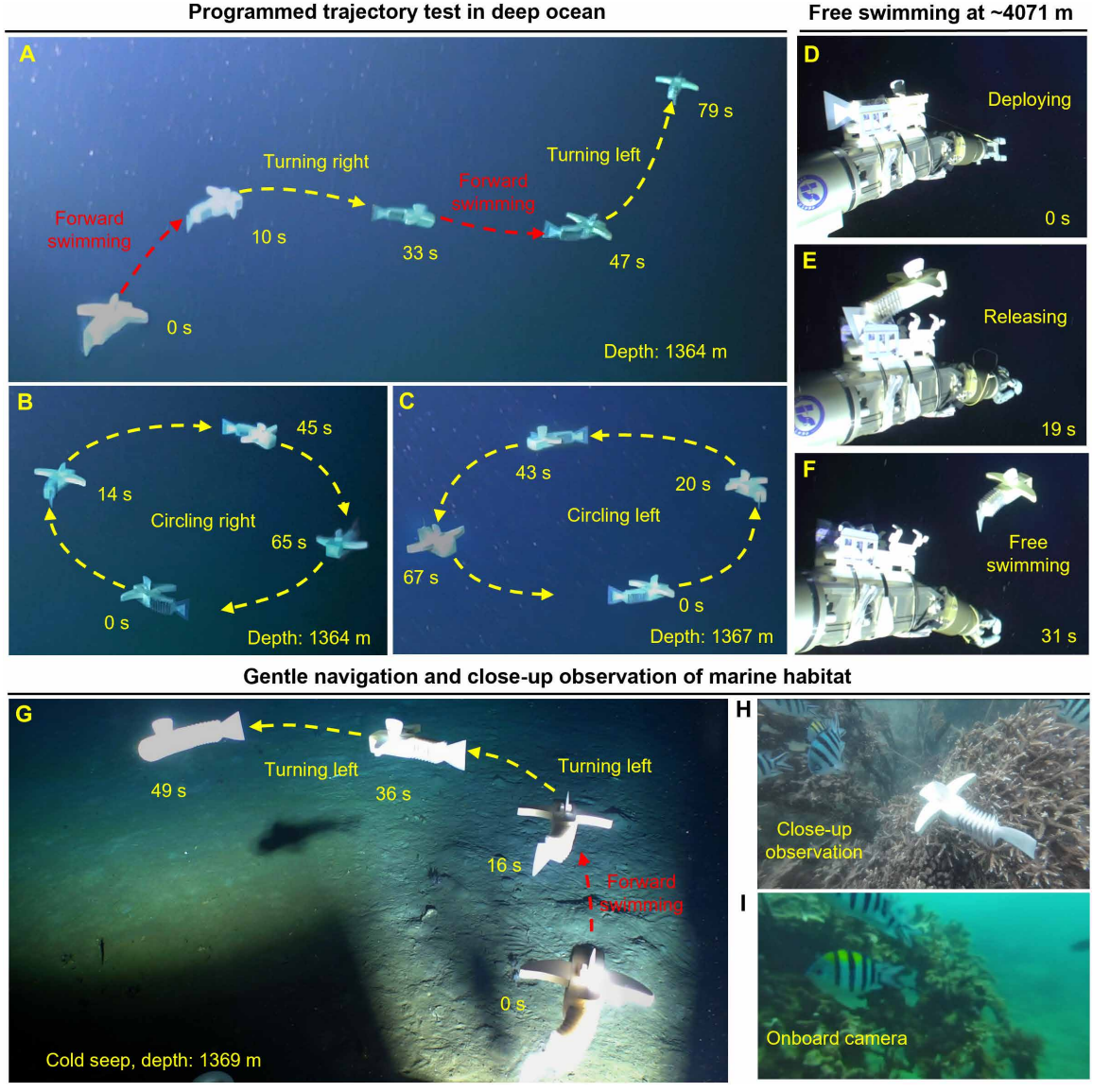

Fig. 6. Deep-sea field test at various depths and close-up observations of marine habitat. (**A** to **C**) Snapshots of the deep-sea field test with preprogrammed multilocomotion (depth of ~1360 m). (**D** to **F**) Deploying and free swimming at a depth of ~4071 m. (**G**) Gentle navigation at the Haima cold seep region (depth of 1369 m). (**H**) Safe interaction and close-up observations of marine habitat. (**I**) Onboard view from the integrated camera.

a robotic arm and demonstrated a maximum free-swimming speed of ~7.2 cm/s (Fig. 6, D to F; fig. S11; and movie S4). The measured speed may be influenced by the dynamic view of the camera and the unsteady flow conditions in the deep sea. This deeper test further confirmed the robot's ability to function and operate under extreme ocean depths, pushing the boundaries of current soft robotics technology. In addition, the potential for the soft robot to cooperate with conventional deep-sea platforms, acting as a wearable or modular enhancement, points to future applications in which soft robots could extend the capabilities of existing exploration systems in a cost-effective and adaptable manner. In terms of practical applications, the robot was able to navigate the delicate Haima cold seep ecosystem at a depth of 1369 m (Fig. 6G and movie S5), completing its tasks with minimal environmental disturbance. Its gentle locomotion enabled it as an ideal tool for in situ investigations, allowing close-up observations of marine life while preserving the integrity of the underwater habitat (Fig. 6, H and I, and movie S6). Building on the ability to conduct low-impact exploration, our robot opens previously unavailable avenues for ecological research and biodiversity studies in deep-sea environments.

CONCLUSIONS

This work presents a generalized strategy to address the critical challenge of soft material stiffening under extreme deep-sea conditions using a broad industrial plasticization approach, enabling the design of deep-sea mobile soft robots with effective actuation. By integrating a liquid dielectric plasticizer into the electrohydraulics, we effectively preserved the softness of the polymer shell while ensuring efficient force transmission for actuation. This dual-function approach is essential in overcoming the performance limitations caused by the low temperatures and high pressures of the deep sea. Moreover, our use of surrounding seawater as alternating positive and negative electrodes, coupled with a cyclic voltage reversal strategy, mitigated charge retention and prevented actuation degradation over time. This enhanced the long-term performance of the soft robot, allowing sustained actuation and multilocomotion swimming at hydrostatic pressures up to 110 MPa. Field tests conducted at depths of ~1360, 3176, and ~4071 m demonstrated the robot's ability to navigate complex trajectories and withstand environmental disturbances, validating its robustness in real-world conditions. Equipped with an optical sensor, the robot continuously monitored and regulated its vertical position, even in turbid conditions, ensuring the precise control near the seabed. These successful demonstrations of multilocomotion, navigation, and advanced sensing technologies in extreme conditions push the boundaries of soft machines. Our work opens possibilities for the development of soft robots capable of performing practical deep-sea missions, setting the stage for future innovations in marine robotics.

MATERIALS AND METHODS

Fabrication of electrohydraulic soft actuators

In the fabrication of electrohydraulic soft actuators, we used PE dielectric films (Shenzhen Zhenhua Adhesive Products Co. Ltd.) with three different thicknesses. Whereas 30-μm-thick and 40-μm-thick PE films were selected to fabricate the electrohydraulic units, a 100-μm-thick PE film was used as a waterproof layer for the electrode. A laser cutter (xTool P2, Makeblock Co. Ltd.) was used to section the plain conductive fabric (Hangzhou Shengneng Packaging Material Co.) into the intended pattern for the electrode, as shown in fig. S1A. After pressing and heat-sealing, 16 identical pouches, each measuring 25 mm in width and 50 mm in height, were fabricated (fig. S1B).

Three different dielectric liquids, PAO (SpectraSyn 2C, Exxon Mobil), FR3 (Cargill), and dimethyl silicone oil (PMX-200 10cSt, Dow Corning Co.), were selected to fabricate electrohydraulic units. Each pouch was filled with 1.1 ml of dielectric liquid. After filling, the pouches were then resealed, including the conductive fabric as the electrode. A completed electrohydraulic laminate is shown in fig. S1C. For the silicone framework, we designed a 3D-printed mold made of polylactic acid (PLA-Lite, Shenzhen Esun Industrial Co. Ltd.) with buoyancy modules arranged inside. Subsequently, the silicone precursor (RTV2-906, Dongguan Tian More Silicone Co. Ltd.) was poured into the mold and cured for 3 hours at 25°C to form the framework (fig. S1D). Two electrohydraulic arrays, referred to as muscle laminates, were then assembled with the silicone framework to construct an electrohydraulic soft actuator (fig. S1, E and F). To determine the number of convolutions, we conducted further experiments to characterize the performance of actuators with 4, 6, 8, and 10 convolutions. Actuated with a voltage of 9 kV at 0.5 Hz, the eight-convolution design achieved maximum actuation angles of 58.32° at 2°C and 64.21° at 25°C, indicating the optimal configuration for propulsion (table S1).

Viscosity characterization

The viscosities of various oils under different temperatures and pressures were characterized, including FR3, PAO, and dimethyl silicone oil. First, a rheometer (Haake Mars 40) was used to obtain the liquid viscosities under different temperatures ranging from 0° to 30°C. During the tests, a conical rotor with diameter of 60 mm was set at a distance of 0.052 mm from the bottom, rotating with the shear rate of 10 s^{-1}. After maintaining a thermal equilibrium at the initial temperature for 5 min, the temperature was increased from 0° to 30°C at a constant rate of 3°C/min. Subsequently, the rheological experiments were conducted with a rheometer (Super HTHP Rheometer 2018, Beijing Institute of Exploration Engineering, China) on PAO, silicone oil, and FR3 to assess their viscosities at pressures ranging from 0 to 110 MPa and a temperature of 25°C. The measurements were performed with an inner cylinder rotor with a diameter of 17.24 mm and height of 38 mm, combined with an outer rotor with a 36.8-mm diameter rotating at 300 rpm. The experimental results indicated a substantial increase in the viscosities of liquids under elevated pressures and lowered temperatures (fig. S2). In contrast, PAO and silicone oil showcased similarly low viscosities. Specifically, the viscosity of PAO was measured as ~64 mPa•s at 100 MPa and 25°C, much lower than that of hydraulic oils used in deep-sea hardware (*41*).

DMA test

A dynamic thermomechanical analyzer (DMA + 1000, Metravib) was used to conduct tensile tests at a frequency of 10 Hz, with the static force and the dynamic force at 0.1 and 0.05 N, respectively. The low-density polyethylene (LDPE) films with thickness of 30 μm (Shenzhen Zhenhua Adhesive Products Co. Ltd.) were cut into rectangular sample strips measuring 30 mm by 50 mm. These samples were then separately immersed in different dielectric liquids for 48 hours. Before the test, the samples were removed from the liquid,

wiped dry, and mounted in a tensile fixture (fig. S3). The environment temperature varied from −10° to 40°C at a heating rate of 3°C/min.

Plasticization ratio characterization

The plasticization ratio was determined by the gravimetric method. Before the experiments, the LDPE films with thickness of 30 μm were cut into 0.2-g pieces, washed with distilled water, and dried in the oven for 20 hours at 60°C. The dried samples were then stored in a vacuum desiccator. During the test, each sample was immersed in ~50 g of PAO, FR3, or dimethyl silicone oil in different sealed containers. Every 8 hours, the samples were removed from the oil and dried between two sheets of filter paper, and their weights were recorded. The plasticization ratio is defined as the ratio of the mass change to the initial value. The results are presented in fig. S4.

Working mechanism of the altitude control module

The altitude control module enabled the robot to autonomously maintain a desired distance from the uneven seabed (fig. S5A). The altitude data were continuously measured with an integrated optical sensor and processed with the MCU. In conjunction with that, the magnetic-driven dorsal fin regulated the altitude to the preprogrammed set point (fig. S5B). This mechanism ensured precisely closed-loop altitude control even in unsteady and turbid underwater conditions.

Fabrication of the soft robot

To ensure its reliable operation under extreme hydrostatic pressures, the optical distance sensor (TOF400C-VL53L1X, Shenzhen Rongtai Hongye Technology Co. Ltd.) was encapsulated with dimethyl silicone oil (PMX-200, 1cst, Dow Corning Co.) for pressure compensation. To mitigate electrostatic interference from the HV in surrounding water, an electronic shield was welded onto the negative electrode of the sensor. In addition, waterproof sealing was achieved by curing the silicone precursor (RTV2-906, Dongguan Tian More Silicone Co. Ltd.) for 3 hours at 25°C (fig. S6A). The encapsulated sensor, along with the electromagnetic dorsal fin, and a battery were integrated on the circuit board and arranged into a 3D-printed mold (fig. S6, B and C). The curing of the silicone precursor for 3 hours at 25°C formed the soft electronic pod that accommodated the onboard power and control systems (fig. S6D). Last, the electrohydraulic actuator was assembled with the electronic pod. The complete deep-sea soft robot is shown in fig. S6 (E and F).

Manufacture and encapsulation of underwater miniature cameras

A miniature camera (EIS40454K) was integrated into the soft robot for underwater investigation. To protect and encapsulate the camera, we coated the lens surface with epoxy resin (Nanya 128), which was subsequently cured at 25°C for 24 hours (fig. S7A). The camera was then assembled with the circuit board to form a camera module. After transferring this module into the mold (fig. S7B), room-temperature vulcanizing silicone (RTV2-906, Dongguan Tian More Silicone Co. Ltd.) was used to fill this mold and allowed to cure at 25°C for 3 hours (fig. S7C). Vulcanized glue was then applied evenly around the camera module for structure sealing, forming the head component of the soft robot (fig. S7D), and the head component was assembled with the body of the soft robot (fig. S7E).

The onboard electronics

The onboard electronic system comprised an MCU, a power management module, an IR receiver, a height control module, and a HV generator, all powered by a 7.4-V lithium-ion battery. A low dropout regulator stepped down the voltage from 7.4 to 3.3 V to power the MCU and other modules. For remote control, an IR receiver was integrated into the circuit. The HV generator operated in three stages. The first stage was a flyback circuit that raised the voltage from 7.4 V to hundreds of volts, primarily consisting of a MOSFET driver (Drv8837), a MOSFET (ST3422A), a transformer (ER11.5 with a turn ratio of 4:400), and several diodes and capacitors. This voltage conversion process was controlled by a signal of pulse width modulation generated by the MCU. The second stage was a voltage-multiplier circuit, which further raised the voltage to 9 kV. In the third stage, a multichannel circuit, primarily consisting of several HV optodiodes (0Z100SG), light-emitting diodes, and MOSFETs (ST3422A), was used to generate sequenced HV signals for propulsion (fig. S8). An optical distance sensor and an electromagnetic dorsal fin were integrated into the altitude control module to regulate the robot's vertical position.

Swimming test under 110 MPa

To further validate the robot's performance under high hydrostatic pressure, the swimming test was conducted in a pressure chamber with an inner diameter of 1.5 m and a depth of 4 m, as shown in fig. S9A. The robot swimming was monitored by a camera that was enclosed in a metallic pressure vessel. First, the robot was installed and fixed with a freely rotatable rod, which was controlled by a stepper motor (fig. S9B). During the experiment, the hydrostatic pressure was increased at a rate of 2 MPa/min until reaching 110 MPa. Before 110 MPa, the robot was fixed in place by the rod. Upon reaching 110 MPa, a command was sent to the motor via an external host computer, releasing the soft robot to complete the free-swimming locomotion (fig. S9C).

Deep-sea field test of the soft robot

The soft robot was deployed by the deep-sea Haima ROV and Haixing ROV (fig. S10A) at various depths. This robot was enclosed in a box mounted on the sampling basket of the Haima ROV and then lowered to the seabed at a depth of 3176 m (fig. S10B). During the field test, an onboard timer activated the embedded voltage amplifier, powering the electrohydraulic actuators. At this point, we remotely controlled the box opening for releasing the robot into seawater (fig. S10C). The robot, actuated with an HV of 9 kV and 0.625 Hz, demonstrated a preprogrammed trajectory tracking and multilocomotion, including forward swimming, turning, and heaving. After the whole process, this robot swam back near the robotic gripper (fig. S10D). Using an optical sensor, the robot could adjust its position on the basis of real-time distance monitoring between itself and the uneven seabed, even in turbid conditions, demonstrating its ability to operate in an unpredictable deep-sea environment. Following a similar procedure, this robot was also deployed and tested at a depth of ~1360 m, including the Haima cold seep region, to confirm its endurance and long-term reliability in deep-sea conditions. For the field test at a depth of ~4071 m, the robot was mounted with a plastic buckle and a clamp on a support attached to the robotic arm (fig. S10E). Upon reaching the target depth, the soft robot was deployed and released via a pull motion executed by the ROV's robotic hand. During the process, the plastic buckle was pulled and

disconnected with a cable. After that, the clamp was opened to release the robot in the deep sea (fig. S10F). More details of the releasing mechanism can be found in fig. S11.

Statistical analysis

In this study, experimental data were collected and analyzed as follows. For actuator performance tests, bending angles were recorded at least three times per condition over five motion cycles using a fixed camera. Sustained actuation was evaluated by recording bending angles every 5 min. Plasticization ratios were measured every 8 hours for up to 72 hours with a minimum of five replicates. Data are presented as mean values with SDs shown as error bars. Swimming speed and turning radius in laboratory tests were measured at least three times. To reduce environmental variability in deep-sea trials, a minimum of five deployment tests were conducted.

Supplementary Materials

The PDF file includes:
Figs. S1 to S11
Table S1

Other Supplementary Material for this manuscript includes the following:
Movies S1 to S6

REFERENCES AND NOTES

1. T. Clarke, Robots in the deep. *Nature* **421**, 468–470 (2003).
2. K. L. Smith, A. D. Sherman, P. R. McGill, R. G. Henthorn, J. Ferreira, T. P. Connolly, C. L. Huffard, A. B. Rover, An autonomous vehicle for long-term monitoring of deep-ocean processes. *Sci. Robot.* **6**, eabl4925 (2021).
3. D. R. Yoerger, A. F. Govindarajan, J. C. Howland, J. K. Llopiz, P. H. Wiebe, M. Curran, J. Fujii, D. Gomez-Ibanez, K. Katija, B. H. Robison, B. W. Hobson, M. Risi, S. M. Rock, A hybrid underwater robot for multidisciplinary investigation of the ocean twilight zone. *Sci. Robot.* **6**, eabe1901 (2021).
4. G. Picardi, M. Chellapurath, S. Iacoponi, S. Stefanni, C. Laschi, M. Calisti, Bioinspired underwater legged robot for seabed exploration with low environmental disturbance. *Sci. Robot.* **5**, eaaz1012 (2020).
5. D. F. Gruber, R. J. Wood, Advances and future outlooks in soft robotics for minimally invasive marine biology. *Sci. Robot.* **7**, eabm6807 (2022).
6. G. Li, T. W. Wong, B. Shih, C. Guo, L. Wang, J. Liu, T. Wang, X. Liu, J. Yan, B. Wu, F. Yu, Y. Chen, Y. Liang, Y. Xue, C. Wang, S. He, L. Wen, M. T. Tolley, A. Zhang, C. Laschi, T. Li, Bioinspired soft robots for deep-sea exploration. *Nat. Commun.* **14**, 7097 (2023).
7. D. Rus, M. T. Tolley, Design, fabrication and control of soft robots. *Nature* **521**, 467–475 (2015).
8. S. I. Rich, R. J. Wood, C. Majidi, Untethered soft robotics. *Nat. Electron.* **1**, 102–112 (2018).
9. R. K. Katzschmann, J. DelPreto, R. MacCurdy, D. Rus, Exploration of underwater life with an acoustically controlled soft robotic fish. *Sci. Robot.* **3**, eaar3449 (2018).
10. R. Baines, S. K. Patiballa, J. Booth, L. Ramirez, T. Sipple, A. Garcia, F. Fish, R. Kramer-Bottiglio, Multi-environment robotic transitions through adaptive morphogenesis. *Nature* **610**, 283–289 (2022).
11. C. A. Aubin, S. Choudhury, R. Jerch, L. A. Archer, J. H. Pikul, R. F. Shepherd, Electrolytic vascular systems for energy-dense robots. *Nature* **571**, 51–57 (2019).
12. N. R. Sinatra, C. B. Teeple, D. M. Vogt, K. K. Parker, D. F. Gruber, R. J. Wood, Ultragentle manipulation of delicate structures using a soft robotic gripper. *Sci. Robot.* **4**, eaax5425 (2019).
13. K. C. Galloway, K. P. Becker, B. Phillips, J. Kirby, S. Licht, D. Tchernov, R. J. Wood, D. F. Gruber, Soft robotic grippers for biological sampling on deep reefs. *Soft Robot.* **3**, 23–33 (2016).
14. B. T. Phillips, K. P. Becker, S. Kurumaya, K. C. Galloway, G. Whittredge, D. M. Vogt, C. B. Teeple, M. H. Rosen, V. A. Pieribone, D. F. Gruber, R. J. Wood, A dexterous, glove-based teleoperable low-power soft robotic arm for delicate deep-sea biological exploration. *Sci. Rep.* **8**, 14779 (2018).
15. S. Licht, E. Collins, M. L. Mendes, C. Baxter, Stronger at depth: Jamming grippers as deep sea sampling tools. *Soft Robot.* **4**, 305–316 (2017).
16. A. Yin, M. Daeffler, R. Shomberg, S. Licht, B. Phillips, "A predictable design and production workflow for field deployable underwater soft actuator applications" in *OCEANS 2024 Singapore* (IEEE, 2024), pp. 1–8.
17. Y. Xu, J. Zhuo, M. Fan, X. Li, X. Cao, D. Ruan, H. Cao, F. Zhou, T. W. Wong, T. Li, A bioinspired shape memory alloy based soft robotic system for deep-sea exploration. *Adv. Intell. Syst.* **6**, 2300699 (2024).
18. F. Pan, J. Liu, Z. Zuo, X. He, Z. Shao, J. Chen, H. Wang, Q. Zhang, F. Yuan, B. Chen, T. Jin, L. He, Y. Wang, K. Zhang, X. Ding, T. Li, L. Wen, Miniature deep-sea morphable robot with multimodal locomotion. *Sci. Robot.* **10**, eadp7821 (2025).
19. G. Li, X. Chen, F. Zhou, Y. Liang, Y. Xiao, X. Cao, Z. Zhang, M. Zhang, B. Wu, S. Yin, Y. Xu, H. Fan, Z. Chen, W. Song, W. Yang, B. Pan, J. Hou, W. Zou, S. He, X. Yang, G. Mao, Z. Jia, H. Zhou, T. Li, S. Qu, Z. Xu, Z. Huang, Y. Luo, T. Xie, J. Gu, S. Zhu, W. Yang, Self-powered soft robot in the Mariana Trench. *Nature* **591**, 66–71 (2021).
20. T. Li, G. Li, Y. Liang, T. Cheng, J. Dai, X. Yang, B. Liu, Z. Zeng, Z. Huang, Y. Luo, T. Xie, W. Yang, Fast-moving soft electronic fish. *Sci. Adv.* **3**, e1602045 (2017).
21. E. Acome, S. K. Mitchell, T. G. Morrissey, M. B. Emmett, C. Benjamin, M. King, M. Radakovitz, C. Keplinger, Hydraulically amplified self-healing electrostatic actuators with muscle-like performance. *Science* **359**, 61–65 (2018).
22. N. Kellaris, V. G. Venkata, G. M. Smith, S. K. Mitchell, C. Keplinger, Peano-HASEL actuators: Muscle-mimetic, electrohydraulic transducers that linearly contract on activation. *Sci. Robot.* **3**, eaar3276 (2018).
23. T. Wang, H.-J. Joo, S. Song, W. Hu, C. Keplinger, M. Sitti, A versatile jellyfish-like robotic platform for effective underwater propulsion and manipulation. *Sci. Adv.* **9**, eadg0292 (2023).
24. Z. Yoder, E. H. Rumley, I. Schmidt, P. Rothemund, C. Keplinger, Hexagonal electrohydraulic modules for rapidly reconfigurable high-speed robots. *Sci. Robot.* **9**, eadl3546 (2024).
25. E. H. Rumley, D. Preninger, A. Shagan Shomron, P. Rothemund, F. Hartmann, M. Baumgartner, N. Kellaris, A. Stojanovic, Z. Yoder, B. Karrer, C. Keplinger, M. Kaltenbrunner, Biodegradable electrohydraulic actuators for sustainable soft robots. *Sci. Adv.* **9**, eadf5551 (2023).
26. T. J. K. Buchner, T. Fukushima, A. Kazemipour, S.-D. Gravert, M. Prairie, P. Romanescu, P. Arm, Y. Zhang, X. Wang, S. L. Zhang, J. Walter, C. Keplinger, R. K. Katzschmann, Electrohydraulic musculoskeletal robotic leg for agile, adaptive, yet energy-efficient locomotion. *Nat. Commun.* **15**, 7634 (2024).
27. S.-D. Gravert, E. Varini, A. Kazemipour, M. Y. Michelis, T. Buchner, R. Hinchet, R. K. Katzschmann, Low-voltage electrohydraulic actuators for untethered robotics. *Sci. Adv.* **10**, eadi9319 (2024).
28. R. Chen, Z. Yuan, J. Guo, L. Bai, X. Zhu, F. Liu, H. Pu, L. Xin, Y. Peng, J. Luo, L. Wen, Y. Sun, Legless soft robots capable of rapid, continuous, and steered jumping. *Nat. Commun.* **12**, 7028 (2021).
29. N. Oikonomeas-Koppasis, P. Schall, Soft matter in the loop. *Nat. Phys.* **19**, 1554–1555 (2023).
30. L. Chen, C. Zhao, J. Huang, J. Zhou, M. Liu, Enormous-stiffness-changing polymer networks by glass transition mediated microphase separation. *Nat. Commun.* **13**, 6821 (2022).
31. E. J. Parry, D. Tabor, Effect of hydrostatic pressure on the mechanical properties of polymers: A brief review of published data. *J. Mater. Sci.* **8**, 1510–1516 (1973).
32. M. S. Paterson, Effect of pressure on Young's modulus and the glass transition in rubbers. *J. Appl. Phys.* **35**, 176–179 (1964).
33. D. R. Mears, K. D. Pae, J. A. Sauer, Effects of hydrostatic pressure on the mechanical behavior of polyethylene and polypropylene. *J. Appl. Phys.* **40**, 4229–4237 (1969).
34. X. Wang, B. Hu, Y. Zhang, C. Cao, G. Li, Compressible dielectric elastomer actuators in high hydrostatic pressures: Models and experiments. *Phys. Rev. E* **110**, L052501 (2024).
35. G. Ding, L. Tam, C. Wu, Molecular investigation on physical and tensile properties of polyethylene (PE) under high-pressure hydrogen environments. *Int. J. Hydrogen Energy* **86**, 1036–1050 (2024).
36. C. Laschi, M. Calisti, Soft robot reaches the deepest part of the ocean. *Nature* **591**, 35–36 (2021).
37. C. Yang, X. Gao, Y. Luo, End-block-curing ABA triblock copolymer towards dielectric elastomers with both high electro-mechanical performance and excellent mechanical properties. *Chem. Eng. J.* **382**, 123037 (2020).
38. B. P. Shtarkyan, I. N. Razinskay, Plasticization mechanism and structure of polymers. *Acta Polym.* **34**, 514–520 (1983).
39. A. K. Saad, F. P. C. Gomes, M. R. Thompson, Plasticizing effect of oxidized biodiesel on polyethylene observed by nondestructive method. *Fuel* **252**, 246–253 (2019).
40. M. Böhning, U. Niebergall, M. Zanotto, V. Wachtendorf, Impact of biodiesel sorption on tensile properties of PE-HD for container applications. *Polym. Test.* **50**, 315e324 (2016).
41. X. Paredes, M. J. P. Comuñas, A. S. Pensado, J.-P. Bazile, C. Boned, J. Fernández, High pressure viscosity characterization of four vegetable and mineral hydraulic oils. *Ind. Crops Prod.* **54**, 281–290 (2014).

Acknowledgments: We acknowledge the support of the following: National Natural Science Foundation of China (52088102, 12472161, and 12102398) and National Key R&D Program of China (grant nos. 2023YFB4704701). The mechatronic equipment is supported by Qingdao

JingYiXuan Technology and Hangzhou CreaCode Technology. **Author contributions:** G.L., T.-W.W., Z.Y., Z.H., A.Z., and T.L. conceived the concept and wrote the manuscript. G.L., P.S., X.L., Z.S., M.L., X.W., Y.C., H. Zhang, B.H., D.C., Z.Z., C.Z., R.W., W.Z., S.N., X.Z., J.-W.W., W.L., H.W., Q. Zhang, Shenlong Wang, H.L., Q. Zeng, and Shiping Wang carried out the experiments. G.L., P.S., X.L., Z.S., X.W., Y.C., H. Zhao, and C.Y. carried out the field tests. G.L., T.-W.W., Z.H., and H. Zhou guided the material and robot fabrication. All authors analyzed and interpreted the data. **Competing interests:** The authors declare that they have no competing interests.

Data and materials availability: The data for this study have been deposited in Dryad with DOI 10.5061/dryad.wm37pvn0t.

Submitted 11 October 2024
Accepted 18 July 2025
Published 13 August 2025
10.1126/scirobotics.adt8054

Science Robotics

Plasticized electrohydraulic robot autopilots in the deep sea

Guorui Li, Peng Shen, Tuck-Whye Wong, Mingyu Liu, Zhenxiang Sun, Xinyu Liu, Yongzai Chen, Xianghan Wang, Hao Zhang, Bingxu Hu, Deli Chen, Zhihan Zhang, Chao Zhang, Rongchen Wang, Wenhao Zhang, Shuai Nie, Xinyue Zhang, Jie-Wei Wong, Haofei Zhou, Wenbo Li, Hao Wang, Qian Zhang, Shenlong Wang, Zhiwen Yu, Hai Li, Hongyu Zhao, Qingyun Zeng, Shiping Wang, Zhilong Huang, Cong Ye, A-Man Zhang, and Tiefeng Li

Sci. Robot. **10** (105), eadt8054. DOI: 10.1126/scirobotics.adt8054

Science Robotics (ISSN 2470-9476) is published by the American Association for the Advancement of Science. 1200 New York Avenue NW, Washington, DC 20005. The title *Science Robotics* is a registered trademark of AAAS.